



Intestinal bacteria trigger a hibernation-like state in homotherms via the gut-brain axis



Ziqiang Bao^{1,2}, Cheng Guo^{1,3}, Yi Chen^{1,2}, Tao Lei³, Hua Peng^{1,3}, Han Zhang^{1,3}, Xiaofei Zhang^{1,3}, Ying Ban⁴, Dunwu Qi⁵, Juntao Feng⁶✉ & Zuofu Xiang^{1,2}✉

The adaptation to low temperature has research value in the fields of spaceflight, disease treatment, and ecological evolution. However, continuous exposure to cold leads to hypothermia and death in homothermic animals. Interestingly, heterothermic animals can easily overcome this challenge. We transferred intestinal bacteria from hibernating *Marmota himalayana* into mice (homothermic animals) and successfully induced a torpor-like state. The mice exhibited typical characteristics of hibernation (torpor-like), such as the rectal temperature decreased by 3.72–4.58 °C, respiration rate and physical activity were down-regulated, and heat was concentrated in the brown adipose tissue. Those were associated with the Sphingolipid metabolism, regulated by *Bacteroides*, opened the temperature switch in the medial preoptic area and ventromedial hypothalamus through the “gut-brain axis”. Our findings suggested that gut bacteria can regulate thermoregulation via the gut-brain axis and induce animals to adapt to low temperatures in a torpor-like state.

How to induce human hibernation by artificial means is an interesting study and it was first proposed in the aerospace field, since low body temperature and low metabolism could alleviate energy consumption and thus better maintain basic biological processes during dormancy¹. Research into hibernation-like states has not only contributed to study the animal over-winter mechanism, but also been applied in treating and delaying disease progression, with therapeutic hypothermia used to address cardiac arrest, brain damage, and organ transplantation^{2,3}. As homeothermic, humans must regulate their internal temperatures to cope with short-term cold pressures and compensate for decreases in body temperature through the neuro-humoral mechanisms^{4,5}. However, continuously low temperatures can lead to hypothermia and potentially death⁶. Therefore, an exogenous approach is necessary to address the challenges of adapting to low temperatures.

Interestingly, heterothermic animals can easily overcome environmental challenges in their natural state^{7,8}. For instance, the body temperature of the Arctic ground squirrel (*Spermophilus parryii*) can drop more than 30 °C during hibernation^{9,10}, and Himalayan marmots (*Marmota himalayana*) are capable of fasting for up to six months in winter while maintaining vitality after emerging from hibernation¹¹. Heterothermic animals

downregulate their body temperature and metabolism and enter hibernation or torpor in winter, thereby reducing energy consumption to adapt to environments with scarce food and low temperatures with no serious damage to the brain, heart, lungs, or other organs¹². Inspired by these adaptations, we were interested in exploring the possibility of replicating the heterothermic mechanisms of hibernation in endotherms, thus enabling the latter to exhibit physiological characteristics similar to hibernation.

Several researches have demonstrated that stimulating endotherms' hypothalamic neurons, body temperature setting point, can induce physiological traits similar to hibernation using ultrasound, injection of drugs, and other methods^{13–15}. That is, appropriate intervention of the central nervous system of endotherms, either via stimulation or protection, is the key to achieving this effect.

Among several known methods to stimulate the central nervous system, the gut-brain axis has garnered significant interest in recent decades. For example, scientists discovered that intestinal bacteria in mice generated neuropeptides that could stimulate the Nod2 receptors in the animals' hypothalamus, regulating body temperature and inducing torpor¹⁶. In other studies, gut microorganisms promoted host adaptation to low temperatures through interaction with thyroid hormones to stimulate thermogenesis in

¹Institute of Evolutionary Ecology and Conservation Biology, Central South University of Forestry and Technology, Changsha, Hunan, China. ²College of Forestry, Central South University of Forestry and Technology, Changsha, Hunan, China. ³College of Life Science and Environment, Central South University of Forestry and Technology, Changsha, Hunan, China. ⁴Ruoergai Wetland National Nature Reserve Administration, Ruoergai Country, Sichuan, China. ⁵Chengdu Research Base of Giant Panda Breeding, Chengdu, Sichuan, China. ⁶Department of Respiratory Medicine, Xiangya Hospital, Central South University, Changsha, China.

✉ e-mail: jtfeng1976@csu.edu.cn; xiangzf@csuft.edu.cn

brown adipose tissue (BAT)^{17–19}. Based on these results, we sought to investigate whether transplantation of the intestinal bacteria from hibernating Himalayan marmots, a kind of heterothermic animal living in the Tibetan plateau region, into endothermic animals could result in a torpor-like state at low temperatures in the new host.

In this study, to observe how the new host adapted to the cold, the intestinal bacteria of wild hibernating Himalayan marmots were transplanted into mice. We hypothesized that the dominant bacteria of the hibernating *Marmota himalayana* could modulate hypothalamic neurons via the gut-brain axis under the cold condition, allowing the host to acclimate to the low temperature by initiating a state similar to hibernation, consistent with the principle of coevolution. Thus, it provides insights and a theoretical foundation for inducing a hibernation-like state in homeothermic animals.

Results

Marmota himalayana experienced hypothermia and hypometabolism during hibernation

The characteristics of hibernation in heterotherms include low body temperature and low metabolism²⁰. To eliminate the interference of the energy reserves on metabolism^{11,21}, we then measured the body weights of marmots during their active period (Fig. 1A, $n = 124$, $Y = 0.47^*X + 3.09$, $p < 0.0001$) and some environmental parameters (Fig. S1), then simulated their weight changes while hibernating in the cave (Fig. 1A, $n = 33$, $Y = -0.34^*X + 9.36$, $p < 0.01$) using post-hibernation and pre-hibernation data, and need to ensure that only animals with similar body weights and body fat compositions were sampled from *Marmota himalayana* during activation group (June–July) and hibernation group (December–January). Finally, it was verified that there were no significant differences in body weights and relative fat contents between the active and hibernating mammals sampled in this experiment (Fig. 1B, C), and the rectal temperatures and respiratory rates were significantly reduced in hibernating animals by 70% and 95%, respectively (Fig. 1D, E).

The temperature at the body surface was measured at the extremities and at the back after removing a patch of hair and exposing the skin (Fig. 1F, blue arrow). Body temperatures in hibernating marmots were significantly lower than those of active marmots at all body locations, and the highest body temperature in hibernating marmots was detected in the brown adipose tissue region (back) rather than the extremities (tail and limbs). This differed from the distributions of body surface temperature in active marmots, where high temperatures were also detected in heads and limbs (Fig. 1G–I). These findings were consistent with the physical characteristics typically found in heterothermic animals during hibernation.

Bacteroides were the dominant bacteria participating in the hibernation process through sphingolipid metabolism

The gut bacteria are known to be involved in the regulation of host energy metabolism^{22,23}. The Shannon indices at both the genus and species levels were lower in hibernating marmots than active animals (Fig. S2A), and both hierarchical clustering and estimated genetic distance indicated distinct differences between the two experimental groups (Fig. S2B, C). These results suggested changes in the composition and structure of microbiota community during hibernation.

At the family level, the Bacteroidaceae were the most abundant bacteria identified in the guts of the Himalayan marmots (Fig. 2A). At the genus level, 2720 bacterial genera were identified with relative richness greater than 0.001% (Fig. 2B), of which 52 were significantly increased in the hibernating marmots (Fig. S3D, fold >2 , $p < 0.05$). Quantitative analysis of the top 10 bacteria at the genus level (39.11% of the whole) indicated that *Bacteroides* were significantly more abundant by 3.85 times during the hibernation period (Fig. 2D).

Changes in intestinal bacteria also cause corresponding changes in metabolites and participate in the regulation of energy metabolism in host animals. At KEGG level 2, we found that only lipid metabolism pathways increased significantly in abundance during hibernation (Fig. S4B). Further

exploration indicated that fatty acid biosynthesis (ko00061) and sphingolipid metabolism (ko00600) pathways were significantly increased among level 3 KEGG pathways (Fig. 2E). We speculated that *Bacteroides uniformis* and *Bacteroides rodentium* were the most likely to play important roles in host adaptation to hypothermia (Fig. 2E).

We also constructed a metabolic network of intestinal bacteria with KEGG metabolic pathways involved in hibernation of *Marmota himalayana* (Fig. S7). We found that 3-oxoacyl-[ACP] synthase III (fabH), beta-galactosidase (lacZ), and phosphoserine phosphatase (serB) were key genes that increased significantly during hibernation and were involved in the synthesis of ceramides (Fig. 3). Therefore, we speculated that the ceramides secreted by *Bacteroides* during hibernation may play key roles in the adaptation of the host to low temperature.

Regulation of sphingolipid metabolism through ganglioside synthesis in the liver and white adipose tissue of *Marmota himalayana*

Since the liver and white adipose tissue (WAT) are the factory and feedstock locations for sphingolipid metabolism^{24,25}, we then analyzed the changes in key sphingolipid metabolism genes during hibernation in *Marmota himalayana*. We found that the *serine phosphatase*, *long chain fatty acid-COA ligase*, and *3-ketodihydrophosphoglycerine reductase* were significantly upregulated in liver and WAT (Fig. 4A–C), providing a substrate for ceramide synthesis during hibernation. Despite the downregulation of *ceramide synthase 4* in liver, *ceramide synthase 4* was significantly increased by 1.61 times in WAT (Fig. 4D), suggesting that WAT was the key organ or tissue in the synthesis of ceramide.

We also analyzed several downstream substances of ceramide and found that *sphingomyelin phosphodiesterase* was significantly downregulated in liver (Fig. 4E), while *ganglioside GM2 activators* were significantly increased in both liver and WAT (Fig. 4F). These findings suggested that ceramide may be involved in animal hibernation and adaptation to low ambient temperature through synthesis of ganglioside (Fig. 4G).

Torpor-like state was triggered by gut bacteria and hypothalamus neurons

To test whether intestinal bacteria from *Marmota himalayana* could induce torpor-like in homothermic animals at low temperatures, we generated ABX mice (Antibiotic-treated mice) to be recipients of fecal transplants (Fig. 5A). Interestingly, we found that cold temperature treatment (Cold group) or transplantation of intestinal bacteria (Bacteria group) alone did not result in reductions of rectal temperatures, but the rectal temperature of transferring the feces and feeding at low temperatures showed decreased by 3.72–4.58 °C on day 5 (Fig. 5B and Fig. S13A, Torpor-like group and Antibiotic group), and exhibited the same characteristics as hibernating Himalayan marmots and other heterotherms, such as the body surface concentrated at the back (Fig. 5C), the respiratory rates and respiratory quotients were decreased (Fig. S13). Those disappeared by garaging Polymyxin beta solution (1:1000) in the Antibiotic group. It was indicated that the intestinal bacteria adapt to low temperatures by inducing host torpor-like.

To further verify whether bacteria act on the hypothalamus, the thermoregulatory center. The c-Fos proteins, a neuronal activation marker, of the Torpor-like group were elevated in the medial preoptic area (MPA) region of the preoptic anterior hypothalamus (POA) and the ventromedial hypothalamus (VMH) region of the posterior hypothalamus (PH) comparing the Cold group (Fig. 5D and Fig. S14A). It was suggested that gut bacteria might induce torpor-like in homothermic hosts through the “gut-brain axis”.

Ganglioside facilitated torpor-like of MPA^{GM2A} and VMH^{GM2A} neurons

Considering the effect of the blood-brain barrier on drug metabolism, we only considered the terminal proteins expression of hypothalamus and the thermoregulation state of recipient mice to explore the specific

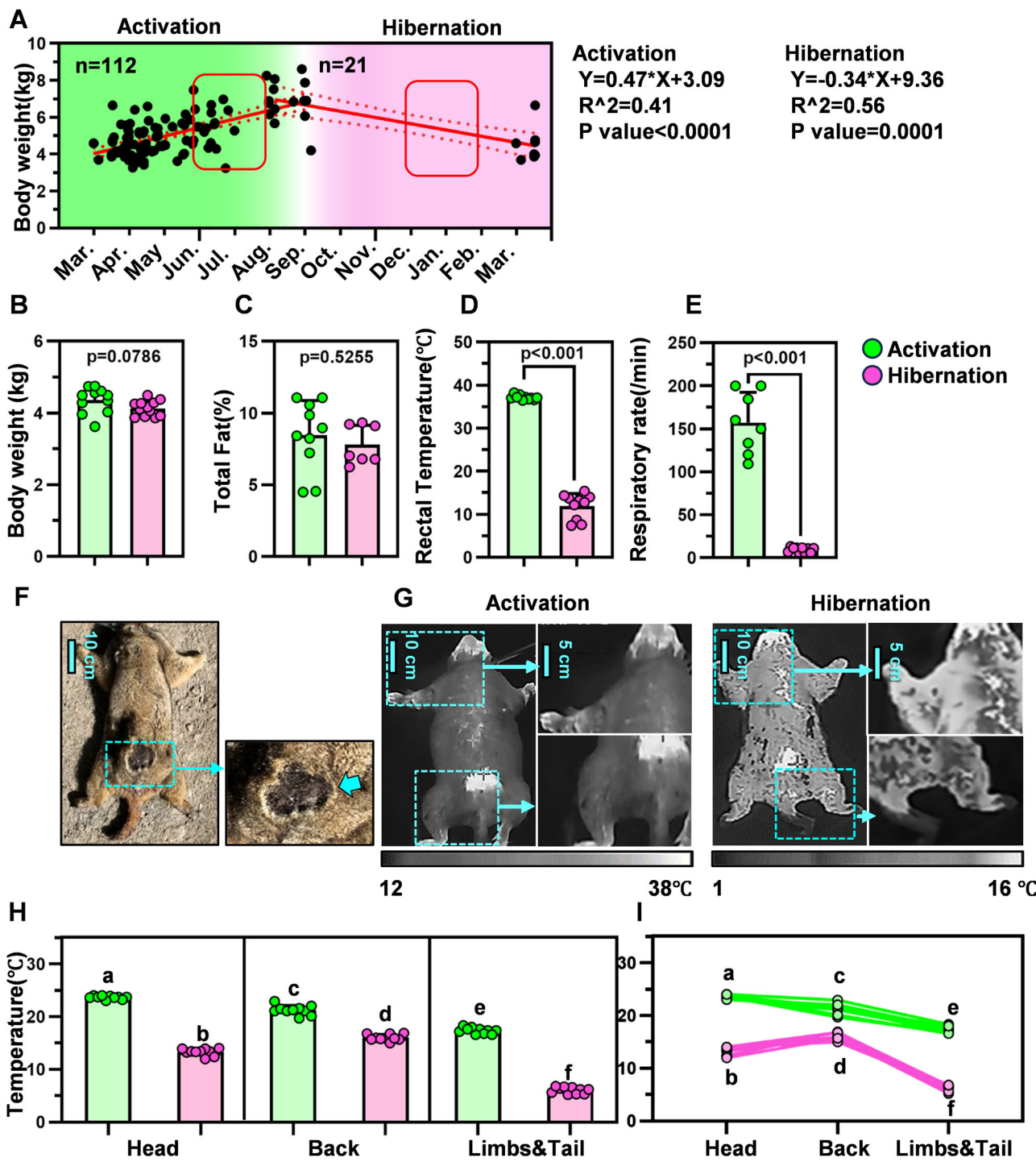


Fig. 1 | Physiological changes in Himalayan marmots during hibernation. **A** Body weight changes in *Marmota himalayana* during the active period (March to September). **B–E** Changes in body weights (B), relative body fat (C), rectal temperatures (D), and respiratory rates (E) of *Marmota himalayana* during their active ($n=11$) and hibernating ($n=11$) periods. **F, G** Photographs (F) and distributions of body surface temperature (G) during the active (left) and hibernation (right) periods

measured using an infrared thermometer. **H, I** The temperatures at the head, back, and limbs and tail of *Marmota himalayana* during the active ($n=11$) and hibernation periods ($n=10$). In the bar graphs, the green and pink bars indicate the active and hibernation periods, respectively. All bar graphs depict means \pm standard errors of the mean. Two-tailed unpaired t-tests (B–E) and Scheffé's one-way ANOVA (H, I) were used to detect statistical significance. * $p < 0.05$, ** $p < 0.01$, *** $p < 0.001$.

neural processes. We first analyzed the preoptic anterior hypothalamus (POA) and found that transient receptor potential cation channel subfamily member 8 (TPRM8) was significantly increased in the peri-ventricular nucleus (Pe) region and medial preoptic nucleus (MPO) region of Torpor-like mice, indicating that cold-sensitive neurons were concentrated in those regions (Fig. 6A, B). To explore whether gut bacteria can regulate body temperature through sphingolipid

metabolism, ceramide synthase (CerS) and ganglioside activator (GM2A) were also used as markers. These were also found to be expressed in the Pe and MPA regions of Torpor-like mice (Fig. 6C, D).

Next, the posterior hypothalamus (PH), the potential downstream brain region of the POA, was tested using the same methodology (Fig. S14A), and found that GM2A was distributed in the VMH, the lateral hypothalamus (LH), and the olfactory tubercle (TU) (Fig. S14B–F). It was

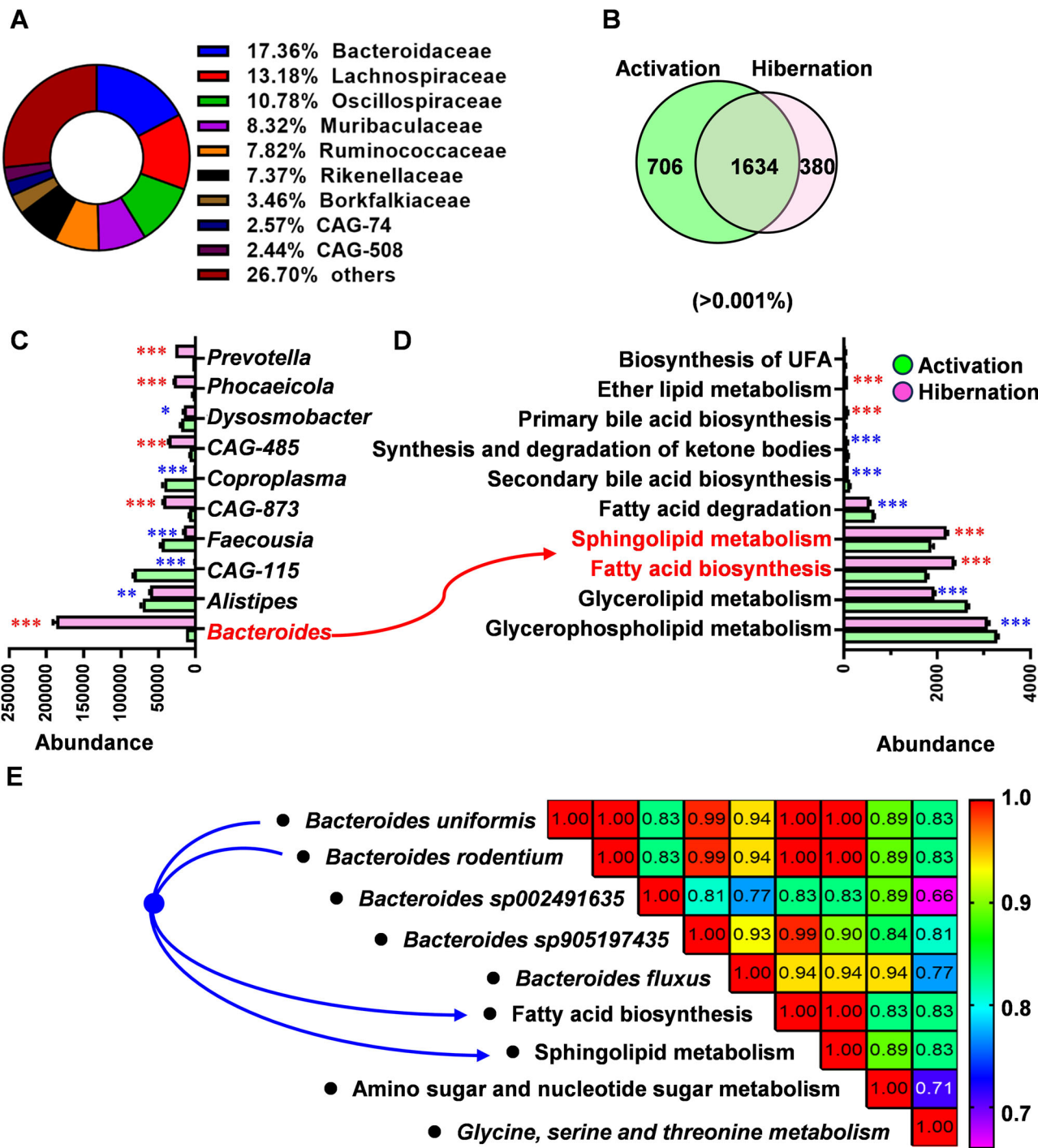


Fig. 2 | Changes in intestinal bacteria during hibernation. A The top 10 relative abundant intestinal bacteria at the family level. B Venn diagram of intestinal bacteria with relative abundance >0.001% at the genus level during the active period (green) and hibernation period (pink). C Bar chart of the top 10 relative abundant bacteria at the genus level in active (green, $n = 3$) and hibernating marmots (pink, $n = 3$). D Bar chart of the top 10 lipid metabolism KEGG pathways (level 3 of KEGG) in active (green, $n = 3$) and hibernating marmots (pink, $n = 3$). E Matrix of Pearson's

correlation coefficients between bacterial taxa and metabolic functions. Strong positive correlations are depicted in red, while strong negative correlations are depicted in purple. The blue arrows indicate the relationships between the dominant bacteria and functions. All bar graphs depict means \pm standard errors of the mean. Two-tailed unpaired t-tests (C, D) were used to detect statistical significance.

* $p < 0.05$, ** $p < 0.01$, *** $p < 0.001$.

preliminarily concluded that sphingolipid metabolism was regulated by MPA^{GM2A} and VMH^{GM2A} in the hypothalamus when considered along with the distributions and tendency (Fig. 6E and Fig. S15).

To test the finally hypothesis, we went on to add antibiotics to inhibit bacterial activity at the starting location of the gut-brain axis. We found that the relative densities of GM2A were separately inhibited by 60.61% and

87.11% in MPA and VMH of the antibiotic group comparing with Torpor-like group (Fig. 7A, B). Correspondingly, the relative CO₂ production, O₂ consumption, the speed and distance traveled were significantly increased after inhibit bacteria (Fig. 7C-E and Fig. S18). Therefore, it intimated those bacteria triggered a torpor-like state via activating sphingolipid metabolism in the hypothalamus and contributing to host adaptation to low temperatures.

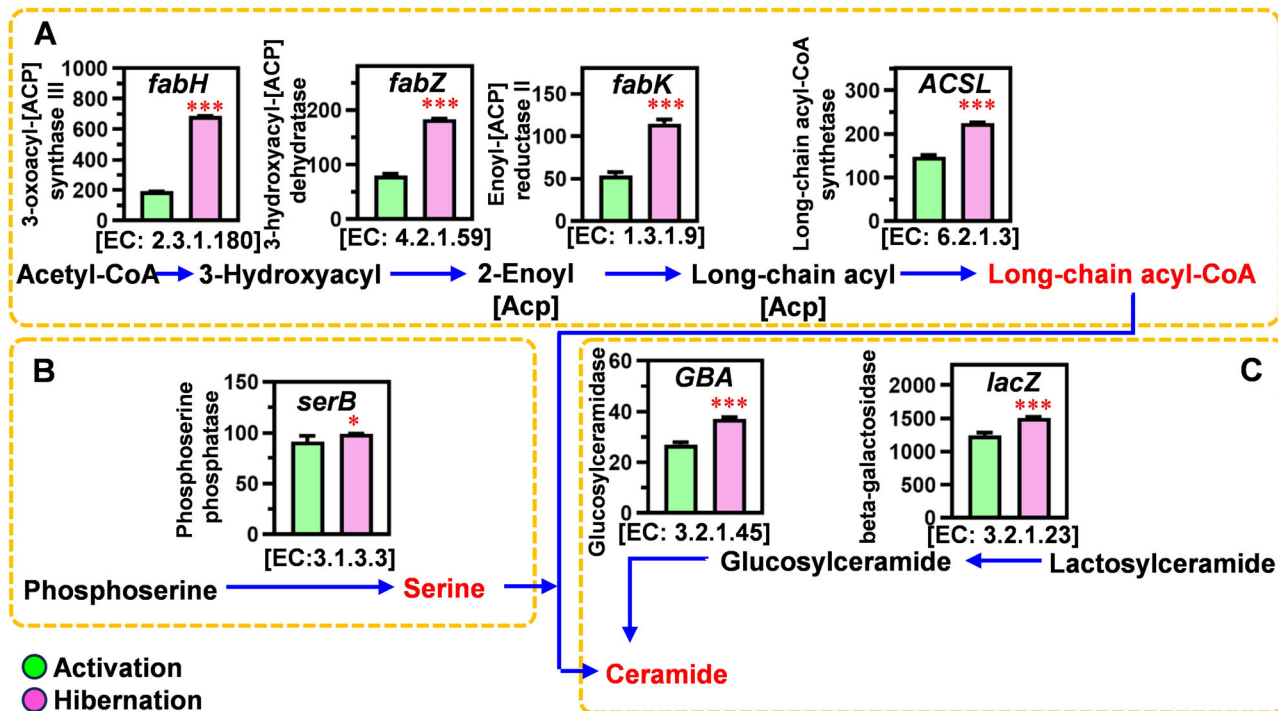


Fig. 3 | Synthesis of ceramides by intestinal bacteria of *Marmota himalayana* during hibernation. Fatty acid biosynthesis (A), serine metabolism (B), and sphingolipid metabolism (C) in intestinal bacteria of active (green, $n = 3$) and hibernating marmots (pink, $n = 3$). All bar graphs depict means \pm standard errors of the mean. Two-tailed unpaired t-tests (A–C) were used to detect statistical

significance. * $p < 0.05$, ** $p < 0.01$, *** $p < 0.001$. fabH 3-oxoacyl-[ACP] synthase III, fabZ 3-hydroxyacyl-[ACP] dehydratase, fabK Enoyl-[ACP] reductase II, ACSL Long-chain acyl-CoA synthetase, serB phosphoserine phosphatase, GBA Glucosylceramidase, lacZ beta-galactosidase.

Discussion

Our experiment revealed that the ceramides secreted by *Bacteroides* actually regulated the energy metabolism in Himalayan marmots during hibernation. The ganglioside, produced downstream of ceramide, was found to promote host low ambient temperature adaptation via the liver and white adipose tissue. This relationship was confirmed via fecal transplantation experiments. Further analysis found that regulation of the hibernation-like state was associated with ganglioside activation in the ganglioside of the medial preoptic area and ventromedial hypothalamus in the hypothalamus.

The first challenge of this study was how to group the Himalayan marmots. Although we were already familiar with their annual life cycles, to maximize physiological differences between active and hibernating marmots and exclude the influence of their own fat reserves on energy metabolism^{11,26,27}, we considered both environmental and individual factors and simulated body weights typically observed during hibernation, which were later confirmed in formal experiments (Fig. 1). At the same time, we found that the animals during hibernation were characterized by low respiratory rates and low body temperatures, with heat mainly concentrated on their backs. Low body temperatures and low respiratory rates contribute to reduced energy consumption rates^{28,29}. In the marmots studied here, the highest surface temperature mainly distributed along their backs where brown adipose tissue (BAT) was localized, rather than other body locations³⁰. This indicated that the marmots produced heat to maintain the body temperature by non-shivering thermogenesis in BAT during hibernation, similar to the Arctic ground squirrel (*Urocitellus parryii*), naked mole-rat (*Heterocephalus glaber*), and Daurian ground squirrel (*Spermophilus dauricus*)^{9,30,31}.

The hypothalamus is the center of body temperature regulation, where both cold-sensitive and heat-sensitive neurons play their critical roles in thermal sensation and signaling conduction^{32,33}. Considering the role of the “gut-brain axis” regulating body energy metabolism³⁴, we hypothesized that the dominant bacteria of the hibernating *Marmota himalayana* could modulate hypothalamic neurons. Metagenomic analysis indicated that

ceramide synthesized by *Bacteroides* was significantly upregulated during hibernation, and ganglioside was synthesized in vivo in the liver and WAT. In this experiment, *Bacteroides uniformis* and *Bacteroides rodentium* were major functional bacteria in *Bacteroides*. Those can encode serine palmitoyl transferase, rate-limiting enzyme for synthesis of sphingolipid, which is converted into 3-ketodihydrophosphingosine and then produced ceramides^{35,36}. In other study has been reported that secondary metabolites of intestinal bacteria regulated host energy metabolism by inhibiting intestinal CerS6 to reduce serum ceramide level³⁷. In addition, our previous research showed that *Marmota himalayana* stored a large amount of unsaturated fatty acids in their liver and white adipose tissue, which were the raw materials for ceramides¹¹. Therefore, we speculated that *Bacteroides* regulated sphingolipid metabolism to help the host adapt to low temperatures.

In accordance with wildlife regulations and the health of the recipient mice, we tested this hypothesis by using ABX mice (Antibiotic-treated mice) as a model for thermoregulation through the gut-brain axis. Interestingly, mice transplanted with fecal samples adapted to low temperatures with reduced metabolism, as evidenced by lower body temperatures, respiratory rates, and respiratory quotient. Temperatures measured at the animals' backs were higher than those measured at other body parts, similar to those of Himalayan marmots during hibernation and returned to normal after treatment with antibiotics (Figs. 1 and 5). Thus, we concluded that the gut bacteria of the Himalayan marmots during hibernation helped their hosts to regulate body temperature for adaption to low temperatures. Further analysis found that expression of MPA^{GM2A} and VMH^{GM2A} in the hypothalamus was significantly higher in torpor-state animals than controls, and the capacities for gas exchange and physical activity were also weakened.

In other studies, MPA and VMH were separately the upstream and downstream brain regions of the hypothalamus, which were rich in temperature-sensing neurons and promoted heat production in brown adipose tissue in the body's extreme low temperature environment^{32,38}. In addition, the ganglioside has the function of activating and repairing neuron by regulating the lipid composition of neuronal membranes^{39–41}. Therefore,

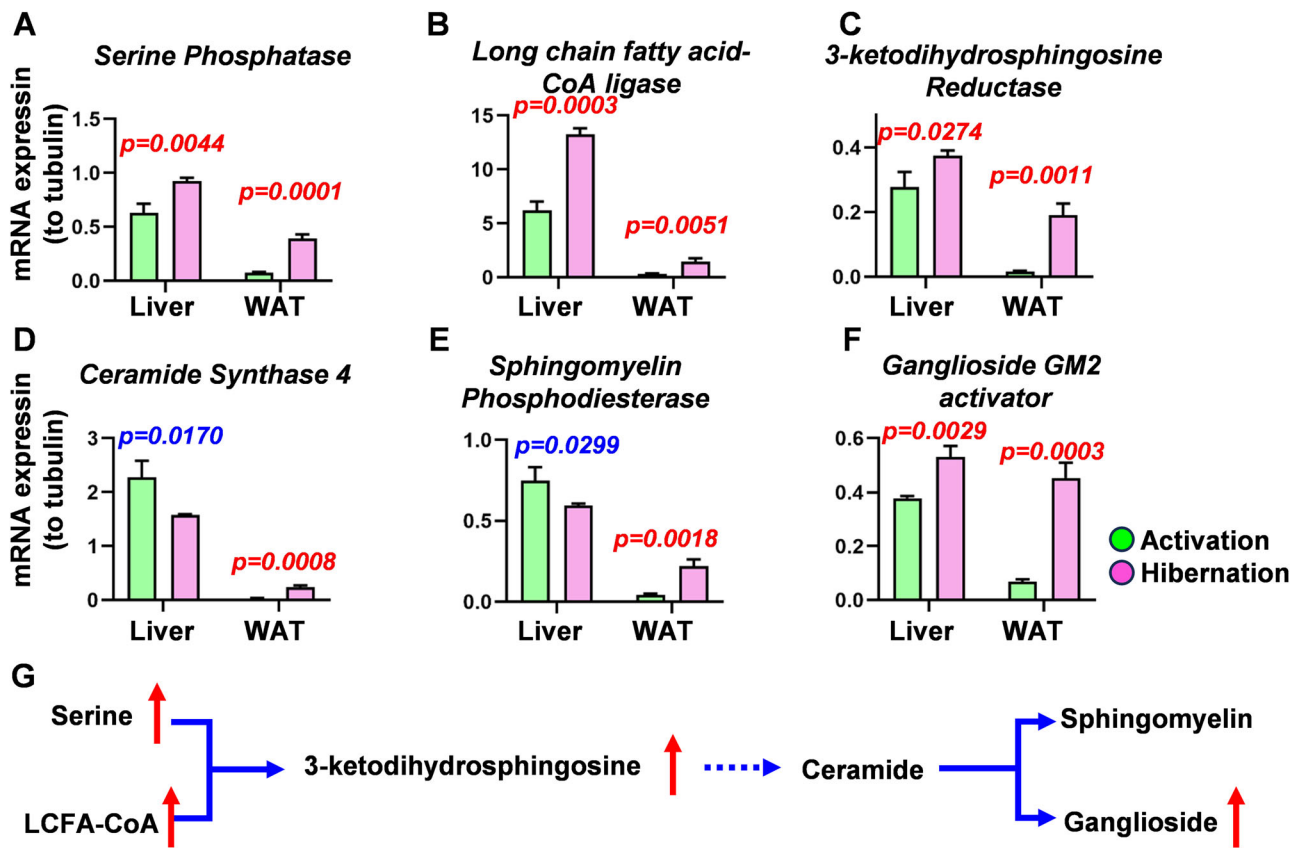


Fig. 4 | The gene expression of key enzymes related to ganglioside synthesis in the liver and white adipose tissue of *Marmota himalayana* during hibernation.

A–F Relative mRNA expression of serine phosphatase (A), long chain fatty acid-CoA ligase (B), 3-ketodihydrosphingosine reductase (C), ceramide synthase 4 (D), sphingomyelin phosphodiesterase (E) and ganglioside GM2 activator (F), as compared to tubulin via RT-qPCR in active (green, $n = 3$) and hibernating marmots (pink, $n = 3$).

G Diagram of ganglioside synthesis. Red arrows indicate parts of the pathway that were significantly upregulated in both liver and WAT (white adipose tissue). In the bar graphs, the green and pink bars indicate the active and hibernation periods, respectively. All bar graphs depict means \pm standard errors of the mean. Two-tailed unpaired t-tests (A–C) were used to detect statistical significance. $^*p < 0.05$, $^{**}p < 0.01$, $^{***}p < 0.001$.

we inferred that ganglioside acted as a protector to maintain the complete neuron structure of MPA and VMH at low temperatures, and those eventually achieved reduce energy metabolism and continuous heat production (Fig. 8).

In conclusion, the sphingolipid metabolism, driven by intestinal *Bacteroides* of hibernation Himalayan marmots, stimulated expression of MPA^{GM2A} and VMH^{GM2A} in the hypothalamus, ultimately helping the host adapt to low temperatures. This research not only explains the temperature regulation mechanism of the Himalayan marmot during hibernation, but might also provide a theoretical basis for the non-invasive induction of body adaptation to low temperatures and reduction of energy expenditures. In the future, we aim to isolate and purify the target bacteria to explore their specific pathways and metabolic processes.

Methods

Experimental design

To identify the key bacteria in hibernating Himalayan marmots, we used active marmots as controls. The selection of marmots according to seasonal environmental conditions was carefully considered. Marmots for the active and hibernating experimental groups were sampled during time periods with maximal differences among environmental conditions, and the weights and relative fat contents of animals from the two experiment groups were kept as similar as possible to eliminate the interference of energy reserves on subsequent analyses.

Data including local monthly temperature, rainfall, and sunshine over the previous ten years were collected (Fig. S1A–D). Environmental conditions in June–July and December–January showed the largest separation in

the principal component analysis plot (Fig. S1E). Daily observations of the natural environment during these two time periods confirmed that environmental conditions were distinct (Fig. S1F). And it was verified by measuring the body weights and body fat between the activation group (June–July) and hibernation group (December–January) (Fig. 1A–C).

Energy metabolism of *Marmota himalayana*

The physical parameters of Himalayan marmots related to energy metabolism were collected after capture. Resting respiratory rates, rectal temperatures (Probe thermometer, Nanjing Suce Measuring Instruments Co., LTD, China, operating temperature range from -50 to $+300$ °C), and body surface temperature (Infrared thermometer, HM-TPH21-3AXF, Hangzhou Haikang micro image sensing Technology Co., LTD, Zhejiang, China) were measured while animals were at rest. In accordance with the method mentioned previously¹¹, the weights of fresh small intestines and total fat contents were measured after intramuscular injection of Zoletil (25 mg/kg, VIRBAC Technology Co., Ltd.) and subsequent dissection.

DNA extraction and metagenomic sequencing

After collecting the feces of marmots from the active group ($n = 3$) and the hibernation group ($n = 3$), fecal surfaces were cleaned using normal saline solution for 3–5 min, and 1–2 g of the core were retained. Genomic DNA was extracted using the E.Z.N.A.® stool DNA Kit (Omega Bio-tek, Norcross, GA, U.S.), and DNA integrity was assessed using the Agilent 5400, per manufacturer's instructions. The TruSeq™ DNA Sample Preparation Kit (Illumina, NEB, USA) and cBot TruSeq PE Cluster Kit v3-cBot-HS were used to construct PE libraries and perform bridge amplification. Sequencing

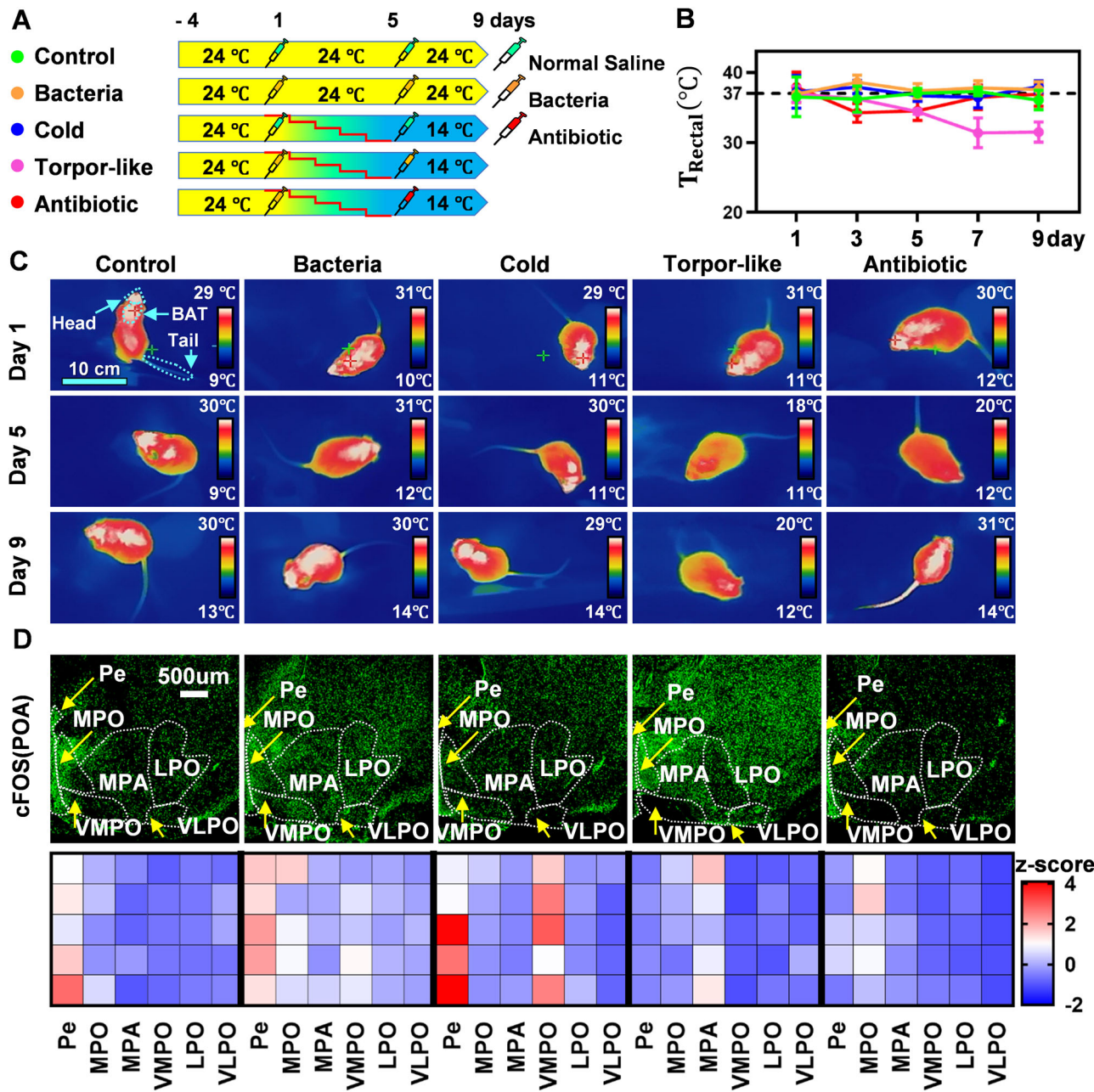


Fig. 5 | Body temperature and hypothalamus neurons in ABX mice after fecal transplantation. **A** Experimental design of fecal transplantation experiment. **B** Rectal temperature changes in mice from day 1 to 9. **C** Images of surface body temperatures of mice as measured by infrared thermometer. **D** Representative immunofluorescence images (top) and z-score heatmap (bottom) of cFOS in the POA (preoptic anterior hypothalamus). In the bar graphs, the green, orange, blue, pink, and red bars indicate the in the Control ($n = 5$), Bacteria ($n = 5$), Cold ($n = 5$),

Torpor-like ($n = 5$), and Antibiotic ($n = 5$) groups, respectively. All bar graphs depict means \pm standard errors of the mean. ANOVA was used to detect statistical significance. $^*p < 0.05$, $^{**}p < 0.01$, $^{***}p < 0.001$. BAT brown adipose tissue, Pe periventricular nucleus, MPO medial preoptic nucleus, MPA medial preoptic area, VMPO ventromedial preoptic nucleus, LPO lateral preoptic area, VLPO ventrolateral preoptic nucleus.

was performed using TruSeq SBS Kit v3-HS reagents and the Paired-End 150 bp mode of the Illumina NovaSeq 6000 instrument at Shanghai Biocenter Biological Technology Co. Ltd. Raw data were uploaded in the National Genomics Data Center (NGDC) of the China National Center for Bioinformation (<https://ngdc.cncb.ac.cn/gsa/>; NGDC: CRA020396).

To ensure the accuracy of bioinformatic analysis, low-quality sequences (illuminaclip: adapters, Fa: 2:30:10 slidingwindow: 4:15, minlen: 75) and host sequences (GenBank: GCA_005280165.1) from the raw sequence data were identified and discarded using trimmomatic v0.36, leaving only clean sequence reads. Then, Megahit v1.1.2-G02102E1 and PlasFlow software were used to assemble contigs (-min-contig-len 500) and

annotate contigs (length ≥ 1000 bp). Genes were predicted and clustered by METAProdigal v2.6.3 (<http://prodigal.org/>) and CD-HIT software (<http://www.bioinformatics.org/cd-hit>, 95% identity, 90% coverage), with the longest gene in each cluster used as the representative sequence to identify the gene in the non-redundant gene catalog. Finally, we used Salmon v1.1.0 (<https://github.com/COMBINE-ab/salmon>) to estimate the abundance of genes.

Microbiome statistical analysis

The Shannon index and the Simpson index were calculated to estimate the alpha diversity of the gut microbiota to indicate the equilibrium state of the

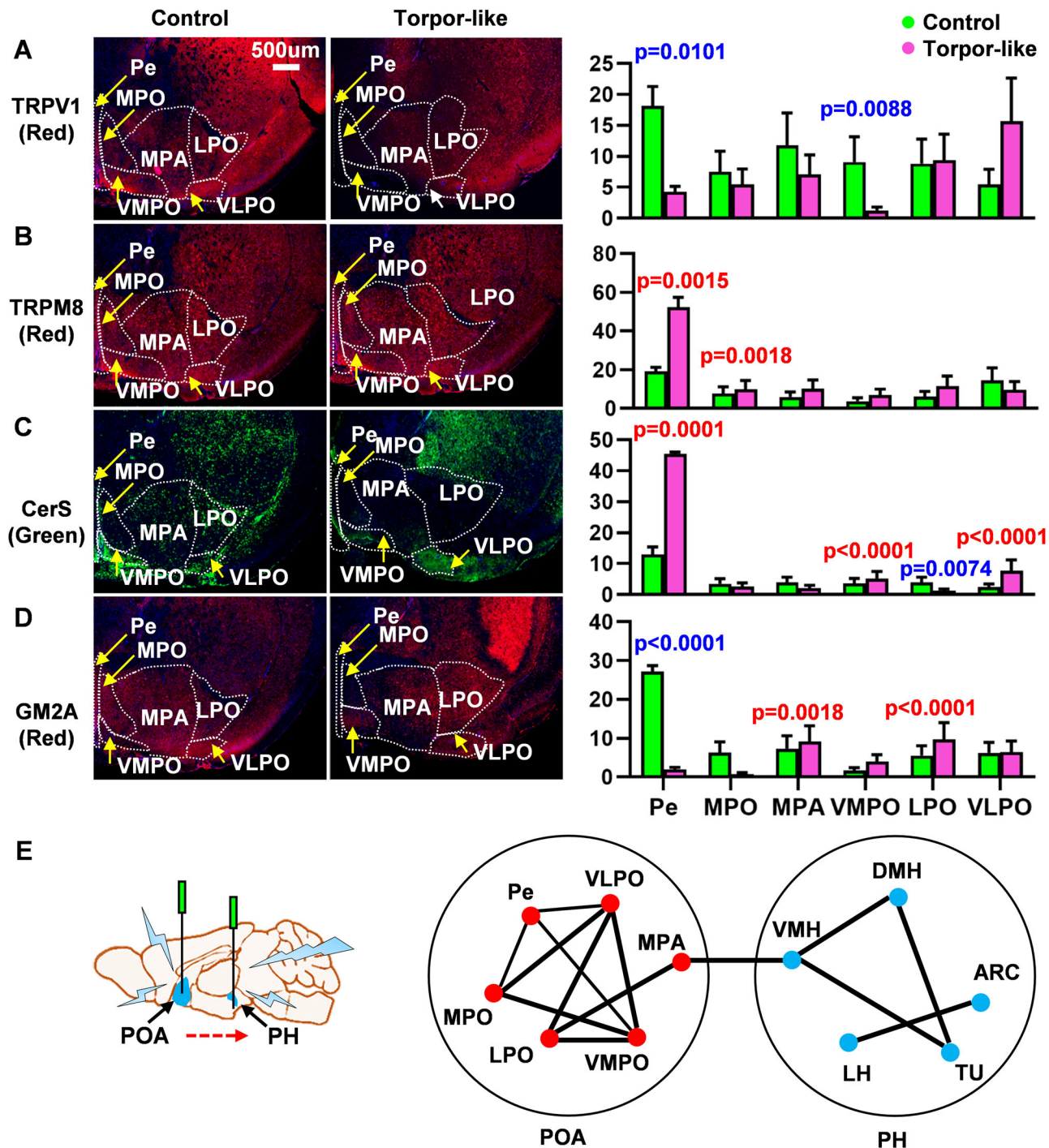


Fig. 6 | The protein expression and distribution in the preoptic anterior hypothalamus of the Control and Torpor-like mice. **A–D** Representative immunofluorescence images (left) and protein densities (right) of TRPV1, TRPM8, CerS, and GM2A in the POA (preoptic anterior hypothalamus) of Control and Torpor-like mice. **E** The relationship between of POA and PH (posterior hypothalamus). In the bar graphs, the green and pink bars indicate the Control ($n=5$) and Torpor-like ($n=5$) groups, respectively. All bar graphs depict means \pm standard errors of the mean. Two-tailed unpaired t-tests (A–D) was used to detect statistical significance.

* $p < 0.05$, ** $p < 0.01$, *** $p < 0.001$. CerS ceramide synthase, GM2A ganglioside activator, TRPM8 transient receptor potential cation channel, subfamily member 8, TRPV1 transient receptor potential vanilloid 1, MPA medial preoptic area, VLPO ventrolateral preoptic nucleus, MPO medial preoptic nucleus, Pe periventricular nucleus, VMPO ventromedial preoptic nucleus, LPO lateral preoptic area, DMH dorsomedial hypothalamus, ARC arcuate nucleus, LH lateral hypothalamus, VMH ventromedial hypothalamus, TU olfactory tubercle.

habitat and living conditions. We calculated those diversity indices using Mothur v.1.30.1 at the genus and species level as well as for KEGG functions (Fig. S2A).

The degree of variation between samples can be assessed by estimating beta diversity in the abundance distributions of species or functions. The Bray-Curtis, Weighted Unifrac, and Unweighted

Unifrac algorithms were used to calculate the distances between pairwise samples to generate a distance matrix and perform hierarchical clustering (Fig. S2B). In the same way, non-metric multidimensional scaling (NMDS), principal component analysis (PCA), and principal co-ordinates analysis (PCoA) were performed to assess the validity of our groupings (Fig. S2C).

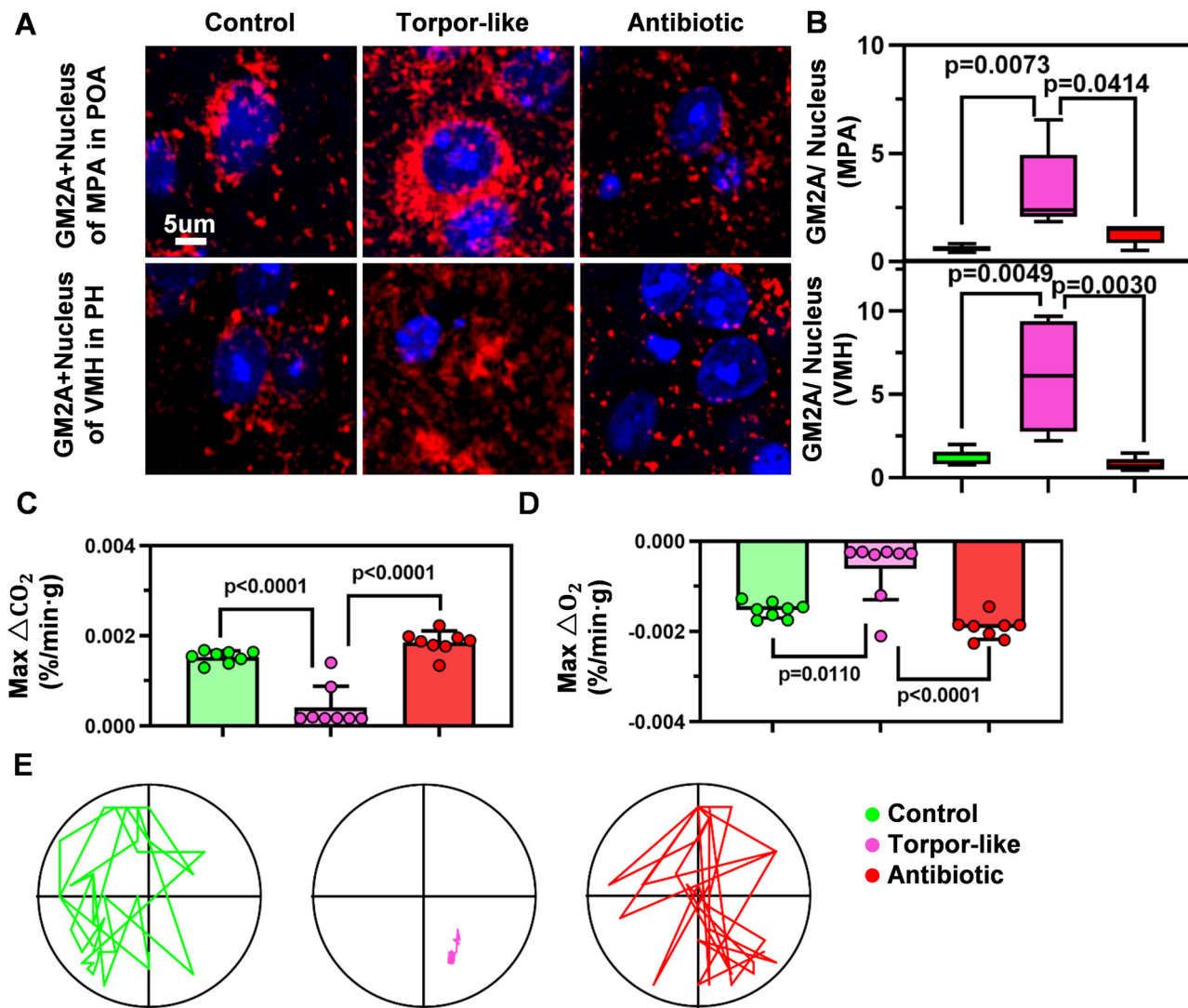


Fig. 7 | Energy metabolism changes after inhibiting bacteria. **A** Representative immunofluorescence images of GM2A protein and nucleus distribution in the Control, Torpor-like, and Antibiotic groups. **B** Relative GM2A expression in MPA (top) and VMH (bottom) of the Control, Torpor-like, and Antibiotic groups. **C, D** Maximum relative release rates of carbon dioxide production (C) and maximum relative release rates of oxygen consumption (D) in Control, Torpor-like, and

Antibiotic treatment groups. **E** Movement trajectories in Control, Torpor-like, and Antibiotic treatment groups. In the bar graphs, the green, pink, and red bars indicate the Control ($n = 5$), Torpor-like ($n = 5$), and Antibiotic ($n = 5$) groups, respectively. All bar graphs depict means \pm standard errors of the mean. ANOVA was used to detect statistical significance. $*p < 0.05$, $**p < 0.01$, $***p < 0.001$.

The taxonomy and abundance of bacteria were analyzed using kraken2 v2.0.6 (–threads 16 –quick –return-zero-counts –Gzp-compressed –paired). All sequences were classified at seven phylogenetic levels (domain, phylum, class, order, family, genus, and species), and relative abundances were estimated using Bracken (<https://ccb.jhu.edu/software/bracken/>).

For predicting the function of bacteria, the Hidden Markov Model algorithm was used to map GeneIDs and KEGG functions (Fig. S3). Annotation and richness were calculated at the levels of genes and biological pathways (E-value cutoff of $1-3 \times 10^{-5}$). Among carbohydrate and amino acid metabolic pathways, amino sugar and nucleotide sugar metabolism (ko00520) and glycine, serine, and threonine metabolism (ko00260) were the most significantly increased in the intestines of hibernating marmots (Fig. S4). The relationships between dominant bacteria and gene expression were ultimately linked using Pearson's correlation coefficients ($p < 0.05$) (Fig. S5).

Detection of gene expression related to sphingolipid metabolism by RT-qPCR

The impacts of hibernation on sphingolipid metabolism in the liver and white adipose tissue (WAT) of *Marmota himalayaan* were assessed via RT-

qPCR. Total RNA was extracted from tissues using the RNAsprep Kit (TIANGEN, Beijing, China), and RNA quality for each sample was assessed using 1% agarose gel electrophoresis. The cDNA templates were synthesized from total RNA using the iScript cDNA Synthesis Kit and the following reaction conditions: 5 min at 25 °C, 30 min at 42 °C, 5 min at 85 °C, and a final hold at 4 °C. Target genes were then amplified using the following reaction: 1 μ L template (0.5 μ g/ μ L), 5 μ L SsoAdvanced™ Universal SYBR® Green Supermix (Bio-Rad, Hercules, CA, USA), 3.5 μ L RNase-free water, 0.5 μ L forward primer, 0.5 μ L reverse primer, and 0.5 μ L cDNA. RT-qPCR (quantitative real-time polymerase chain reaction) was then performed as follows: initial denaturation at 95 °C for 60 s and 40 cycles of denaturation at 95 °C for 5 s, annealing at 55 °C for 30 s, and extension at 72 °C for 30 s. Each sample was assayed in triplicate, and the relative mRNA expression was quantified using the $2^{-\Delta\Delta CT}$ (cycle threshold) method using *tubulin* as the reference gene (Table 1).

Drug susceptibility test

Drug susceptibility tests were performed in accordance with the methods of Bao et al.¹¹. Bacterial dilutions (1:1000) were made from active and

hibernation group samples, added to drug-sensitive test papers (Hunan Bkman Biotechnology Co., LTD), and incubated at 37 °C for 3 days. The radii of the antibacterial rings were then measured (Fig. S8A). Twenty and two antibiotics were found to inhibit bacteria in the active group and hibernation groups, respectively (Fig. S8B). Polymyxin beta (Anhui Zhongding Animal Pharmaceutical Co., LTD) was the only antibiotic found

to be effective only against bacteria from the hibernation group (Fig. S8C). Thus, Polymyxin beta was used for the fecal transplantation experiments.

Fecal transplantation experiment

To explore the effects of bacteria from hibernating mammals on energy metabolism of hosts at low temperature (Fig. 9), 25 healthy ABX mice (Antibiotic-treated mice) were randomly divided into five groups and acclimated to experimental conditions at 24 °C for 4 days before fecal transplantation (“pre-experiment”). No differences in energy metabolism and growth were found between groups and sex in the pre-experiment period (Figs. S9 and S10). In the formal experiment, the Control group and the Bacterial group were reared at 24 °C, and either normal saline or a fecal dilution (1:1000) from hibernating Himalayan marmots were administered intragastrically for a period from 1 to 9 days (0.2 mL/d).

The ambient temperatures of the other groups were gradually decreased from 24 °C to 14 °C (1 °C/12 h). The Cold group, the Torpor-like group, and the Antibiotic group were given normal saline, the fecal dilution, and the fecal dilution, respectively (0.2 mL/d). The Antibiotic group were gassed Polymyxin beta solution (1:1000, 0.2 mL/d) after the 5th day (Fig. 5A). The food and water consumption, feces and urine production, huddling behavior, physical parameters (body weight and body length), temperature parameters (T_{rectal} , T_{BAT} , T_{tail} , temperature distribution), respiratory parameters (respiratory rate, respiratory quotient, oxygen consumption, and carbon dioxide production), and activity parameters (movement trajectory, speed, and location) were recorded for each group during the experimental period (Fig. S16 and 17).

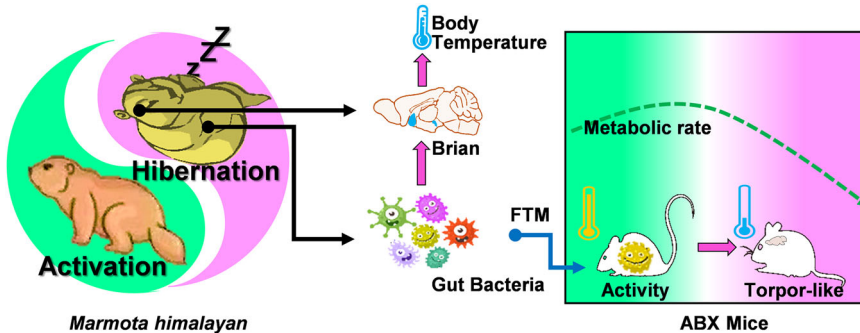
Huddling behavior of mice

For social animals, huddling behavior helps reduce their surface area and slows the rate of individual energy expenditure loss at low temperatures⁴². To quantify the huddling behavior of mice, we measured the distance between the occipital bones of five mice per group (Fig. S11). Lower values indicated that mice were closer together.

Table 1 | The sequences of primers

Gene	Product length (bp)	Annealing temperature (°C)	Sequences (5' → 3')
tubulin	848	59.95	F:GAAGTGGAGACGTGGAAAGG R: TGTCCGAGCATACATTGAGG
serine phosphatase	507	59.93	F:TGGATTATGATGAGTGCCAAACC R: TCTGAATCTGGAAGTCCCCG
long-chain-fatty-acid-CoA ligase	917	60.14	F:GACGACCTCAAGGTGCTTC R: AGAGCAATGCCCTTGACCTG
3-ketodihydrophosphingosine reductase	331	61.48	F:CTCTACATGGGTCTCCGCTCATC R: GTGATAGTCCTGCGCAGTTGA
ceramide synthase 4	270	59.28	F:GGAAAATTACCAAACCAAGACCTG R: AAGCGCGTGTAGTTGAAACATC
sphingomyelin phosphodiesterase	884	60.32	F: TGCTGAGGATCGAGGAGACA R: TGGCCATGAAAGGACAGCAG
ganglioside GM2 activator	1000	60.12	F:GCTCCTTCTGCTCACCGAT R: GCTGGCTCTGGGTCAAGAT

Fig. 8 | Mechanistic model for the regulation of temperature by bacteria through the gut-brain axis.



Thermoregulation of mice

Temperature is the most intuitive parameter to measure changes in mammalian energy metabolism. The smaller the difference between body surface temperature and environmental temperature, the slower the energy loss rate of the species. As with the Himalayan marmots, we continually used a Probe thermometer and Infrared thermometer to measure rectal temperatures and body surface temperatures, respectively. According to the characteristic of higher temperatures in the interscapular regions than the heads, we indicated that the animals generated heat through brown adipose tissue (BAT).

Respiratory parameters of mice

Respiration is another standard for assessing animal energy metabolism. As the oxidation of glucose and lipids are inseparable from oxygen, a more intense reaction process results in the release of greater amounts of energy. We measured the respiratory rates of resting mice during daily feeding. The concentrations of CO_2 and O_2 in the confined space (CLAMS, Columbus, USA) were measured in open or closed cylindrical containers (bottom diameter: 10 cm, height: 15 cm). Before measurement, the maximum amount of oxygen in the containers and the measurement times were screened by burning alcohol and placing healthy mice in the containers. The O_2 consumption rates were not found to fluctuate significantly after the closed 270 s (Figs. S16 and S17).

Activity parameters of mice

Exercise also produces energy expenditure. As oxygen is gradually reduced in a closed environment, animals with low metabolisms are expected to better adapt to low oxygen levels, resulting in behavioral changes. Through statistical analysis of the relationship between the mouse's standing behavior, movement tracks, movement speed, position, and time in the container, we found that mice displayed adaptation to the open environment (from -180 s to 0 s). When the environment was closed, exploration and movement increased again, but mice again adapted to the environment (from 90 s to 270 s, red arrow) (Fig. S17C and S17D). Therefore, measurement of activity parameters in mice was performed between 90 and 270 seconds for this experiment.

Detection of gene expression in the brain by immunofluorescence

To obtain frozen sections of mice brain tissues, the mice were anesthetized with Zoletil (0.05 ml/g) and then dissected. Normal saline (50–100 ml) was perfused into the apex of the heart (left ventricle), and then the right auricle was cut open. A 4% paraformaldehyde fixative solution (30–50 ml) was injected after the liver turned white. The brain tissue was removed and soaked in 4% paraformaldehyde overnight at a low temperature, then washed with phosphate buffer saline and cryoprotected in 30% sucrose. The whole brain was placed on a sample tray and processed by a frozen microtome ($T_{\text{machine}} = -20^{\circ}\text{C}$, $T_{\text{blade}} = -18^{\circ}\text{C}$, slice thickness = 40 μm , Leica, Shanghai, China). The bregma from 4.75 to 0.5 mm were continuously collected, covering the entire hypothalamic region^{32,43–45}.

The brain slices were soaked in phosphate buffer saline. They were then individually permeabilized and blocked in 0.1% Triton X-100 for 1 h and BSA at room temperature for 2 h. Immunofluorescence sections were incubated overnight at 4 $^{\circ}\text{C}$ with the following primary antibodies: cFos (1:500), TRPV1 (1:400), TRPM8 (1:200), CerS (1:200), and GM2A (1:200). Samples were then incubated with fluorescently binding secondary antibody: goat anti-rabbit IgG horseradish peroxidase (1:400) for 50 min. Finally, the fluorescence intensity of cFos protein and cell nuclei (DAPI) in the samples was captured using a fluorescence microscope (excitation wavelength) (Fig. 5D and S14A), and the distributions and densities of target proteins in each brain region were measured using ImageJ (version 1.8.0).

Quantification and statistical analysis

All data are expressed as means \pm standard errors (SD) with three or more independent replicates. Statistical analyses were performed using GraphPad Prism Software (version 10.1.0, GraphPad Software Inc., San Diego, CA,

USA) and R studio (version 1.2.5033, University of Auckland, New Zealand) using ANOVA and t-tests. The threshold for significance was set at $p < 0.05$.

Ethics approval and consent to participate

All experimental protocols adhered to Chinese legal requirements and were approved by the Central South University of Forestry and Technology's Institutional Animal Care and Use Committee (protocol no. 2012-018).

Data availability

The raw data were uploaded in the National Genomics Data Center (NGDC) of the China National Center for Bioinformation (<https://ngdc.cncb.ac.cn/gsa/>; metagenomic sequence: CRA020396, statistical chart data: OMIX009981).

Received: 2 May 2025; Accepted: 3 November 2025;

Published online: 17 December 2025

References

1. Hisanori, F. The effect of low temperatures on environmental radiation damage in living systems: Does hypothermia show promise for space travel?. *Int. J. Mol. Sci.* **21**, 1–11 (2020).
2. Paolo, M. & Sudhin, T. Hippocampus and hypothermia: A missing link. *Developmental Med. Child Neurol.* **65**, 303–304 (2022).
3. Torkjel, T. & Gary, C. Physiological impact of hypothermia: The good, the bad, and the ugly. *Physiol. (Bethesda)* **37**, 69–87 (2021).
4. Søberg, S. et al. Altered brown fat thermoregulation and enhanced cold-induced thermogenesis in young, healthy, winter-swimming men. *Cell Rep. Med.* **2**, 1–24 (2021).
5. Giorgia, G. A conceptual framework to integrate cold-survival strategies: torpor, resistance and seasonal migration. *Biol. Lett.* **18**, 20220050 (2022).
6. Paal, P. et al. Accidental hypothermia: 2021 update. *Int. J. Environ. Res. Public Health* **19**, 25 (2022).
7. Grabek, K. et al. Genetic variation drives seasonal onset of hibernation in the 13-lined ground squirrel. *Commun. Biol.* **2**, 13 (2019).
8. Madeleine, S. et al. Suppression of neurons in circumventricular organs enables months-long survival without water in thirteen-lined ground squirrels. *Science* **386**, 1048–1055 (2024).
9. Rice, S. et al. Omega 3 fatty acids stimulate thermogenesis during torpor in the Arctic ground squirrel. *Sci. Rep.* **11**, 14 (2021).
10. Fritz, G. *Ecological Physiology of Daily Torpor and Hibernation*. Springer Nature Switzerland: Springer Cham (2021).
11. Bao, Z. et al. Fatty acid metabolism and insulin regulation prevent liver injury from lipid accumulation in Himalayan marmots. *Cell Rep.* **42**, 1–14 (2023).
12. Chmura, H. et al. Effects of spring warming on seasonal neuroendocrinology and activation of the reproductive axis in hibernating Arctic ground squirrels. *Integr. Comp. Biol.* **62**, 1012–1021 (2022).
13. Domenico, T., Christopher, J. & Shaun, F. Central activation of the a1 adenosine receptor (A1AR) induces a hypothermic, torpor-like state in the rat. *J. Neurosci.* **33**, 14512–14525 (2013).
14. Yang, Y. et al. Induction of a torpor-like hypothermic and hypometabolic state in rodents by ultrasound. *Nat. Metab.* **5**, 789–803 (2022).
15. Zhao, Z. et al. A hypothalamic circuit that controls body temperature. *Proc. Natl. Acad. Sci.* **114**, 2042–2047 (2017).
16. Ilana, G. et al. Bacterial sensing via neuronal Nod2 regulates appetite and body temperature. *Science* **376**, 1–13 (2022).
17. Khakisahneh, S. et al. Gut microbiota and host thermoregulation in response to ambient temperature fluctuations. *mSystems* **5**, e00514–e00520 (2020).
18. Li, B. et al. Microbiota depletion impairs thermogenesis of brown adipose tissue and browning of white adipose tissue. *Cell Rep.* **26**, 2720–2737 (2019).

19. Sylvain, G. et al. Lipidomics reveals seasonal shifts in a large-bodied hibernator, the brown bear. *Front. Physiol.* **10**, 1–14 (2019).
20. Kelly, L. et al. Opportunities and barriers to translating the hibernation phenotype for neurocritical care. *Front. Neurol.* **14**, 1009718 (2023).
21. Jin, L. et al. Dynamic chromatin architecture of the porcine adipose tissues with weight gain and loss. *Nat. Commun.* **14**, 19 (2023).
22. Luo, T. et al. Crosstalk between innate immunity and rumen-fecal microbiota under the cold stress in goats. *Front. Immunol.* **15**, 1363664 (2024).
23. Ko, C. et al. Regulation of intestinal lipid metabolism: current concepts and relevance to disease. *Nat. Rev. Gastroenterol. Hepatol.* **17**, 169–183 (2020).
24. Zhang, S. et al. Dietary fiber-derived short-chain fatty acids: A potential therapeutic target to alleviate obesity-related nonalcoholic fatty liver disease. *Obes. Rev.* **22**, e13316 (2021).
25. Zhu, C. et al. Insights into the roles and pathomechanisms of ceramide and sphingosine-1-phosphate in nonalcoholic fatty liver disease. *Int. J. Biol. Sci.* **19**, 311–330 (2023).
26. Zhou, S. et al. Effects of human activity on the habitat utilization of Himalayan marmot (*Marmota himalayana*) in Zoige wetland. *Ecol. Evolution* **11**, 8957–8968 (2020).
27. Guo, C. et al. Variation in escape response of Himalayan marmots (*Marmota himalayana*) under different human disturbances. *Ethology* **128**, 143–151 (2021).
28. Rune, S. et al. State dependence of arousal from torpor in brown long-eared bats (*Plecotus auritus*). *J. Comp. Physiol. B* **192**, 815–827 (2022).
29. Nathaniel, E. et al. Nesting box imager: Contact-free, real-time measurement of activity, surface body temperature, and respiratory rate applied to hibernating mouse models. *PLoS Biol.* **17**, 1–13 (2019).
30. Yuki, O. et al. Characterization of brown adipose tissue thermogenesis in the naked mole-rat (*Heterocephalus glaber*), a heterothermic mammal. *Sci. Rep.* **10**, 19488 (2020).
31. Yan, X. et al. Differential protein metabolism and regeneration in gastrocnemius muscles in high-fat diet fed mice and pre-hibernation Daurian ground squirrels: A comparison between pathological and healthy obesity. *Zool. Stud.* **60**, 1–18 (2021).
32. Zhou, Q. et al. Hypothalamic warm-sensitive neurons require TRPC4 channel for detecting internal warmth and regulating body temperature in mice. *Neuron* **111**, 387–404 (2023).
33. Kyoko, T. et al. Somatostatin neurons in prefrontal cortex initiate sleep-preparatory behavior and sleep via the preoptic and lateral hypothalamus. *Nat. Neurosci.* **26**, 1805–1819 (2023).
34. Zhang, Y. et al. Porcine gut microbiota in mediating host metabolic adaptation to cold stress. *NPJ Biofilms Microbiomes* **8**, 1–14 (2022).
35. Eric, B. et al. Bacteroides-derived sphingolipids are critical for maintaining intestinal homeostasis and symbiosis. *Cell Host Microbe* **25**, 668–680 (2019).
36. Luo, J. et al. Lipids regulate peripheral serotonin release via gut CD1d. *Immunity* **56**, 1533–1547 (2023).
37. Zhou, S. et al. A symbiotic filamentous gut fungus ameliorates MASH via a secondary metabolite-CerS6-ceramide axis. *Science* **388**, 1–13 (2025).
38. Feng, C. et al. Cold-sensitive ventromedial hypothalamic neurons control homeostatic thermogenesis and social interaction-associated hyperthermia. *Cell Metab.* **34**, 888–901 (2022).
39. Andrés, F. et al. GM2 gangliosidoses: Clinical features, pathophysiological aspects, and current therapies. *Int. J. Mol. Sci.* **21**, 1–27 (2020).
40. Inamori, K. & Inokuchi, J. Roles of gangliosides in hypothalamic control of energy balance: new insights. *Int. J. Mol. Sci.* **21**, 1–17 (2020).
41. Guo, Z. Ganglioside GM1 and the Central Nervous System. *Int. J. Mol. Sci.* **24**, 1–32 (2023).
42. Qi, X. et al. Adaptations to a cold climate promoted social evolution in Asian colobine primates. *Science* **380**, 1–14 (2023).
43. Zu, S. et al. Single-cell analysis of chromatin accessibility in the adult mouse brain. *Nature* **624**, 378–389 (2023).
44. Shi, H. et al. Spatial atlas of the mouse central nervous system at molecular resolution. *Nature* **622**, 552–561 (2023).
45. Liu, H. et al. Single-cell DNA methylome and 3D multi-omic atlas of the adult mouse brain. *Nature* **624**, 366–377 (2023).

Acknowledgements

This study was supported by the National Natural Science Foundation of China (32171487), the State Forestry and Grassland Administration Bureau of China (2019076079), postdoctoral research grants at the Central South University of Forestry and Technology (45220003), and Hunan Natural Science Foundation (2025JJ60191). The funders had roles in the study design, data collection and analysis, decision to publish, or preparation of the manuscript.

Author contributions

Z.X., Z.B., and C.G. designed the research. Z.X. and Y.B. provided the resources. Z.B., Y.C., T.L., H.P. and H.Z. performed the research. Z.B. and X.Z. analysed the data. All authors discussed the data. Z.B. and Y.C. wrote the manuscript. Z.B., Y.C., C.G., D.Q., J.F. and Z.X. revised the manuscript.

Competing interests

The authors declare no competing interests.

Consent to participate

All authors agreed with the above statement and identified all risks and benefits.

Additional information

Supplementary information The online version contains supplementary material available at <https://doi.org/10.1038/s41522-025-00856-x>.

Correspondence and requests for materials should be addressed to Juntao Feng or Zuofu Xiang.

Reprints and permissions information is available at <http://www.nature.com/reprints>

Publisher's note Springer Nature remains neutral with regard to jurisdictional claims in published maps and institutional affiliations.

Open Access This article is licensed under a Creative Commons Attribution-NonCommercial-NoDerivatives 4.0 International License, which permits any non-commercial use, sharing, distribution and reproduction in any medium or format, as long as you give appropriate credit to the original author(s) and the source, provide a link to the Creative Commons licence, and indicate if you modified the licensed material. You do not have permission under this licence to share adapted material derived from this article or parts of it. The images or other third party material in this article are included in the article's Creative Commons licence, unless indicated otherwise in a credit line to the material. If material is not included in the article's Creative Commons licence and your intended use is not permitted by statutory regulation or exceeds the permitted use, you will need to obtain permission directly from the copyright holder. To view a copy of this licence, visit <http://creativecommons.org/licenses/by-nc-nd/4.0/>.

© The Author(s) 2025